Applications of the Schwinger Multichannel Method with Pseudopotentials to Electron Scattering from Polyatomic Molecules I. Elastic Cross Sections

Alexandra P. P. Natalense, Márcio T. do N. Varella,
Instituto de Física Gleb Wataghin,
Universidade Estadual de Campinas, UNICAMP,
13083-970 Campinas, São Paulo, Brazil

Márcio H. F. Bettega,
Departamento de Física, Universidade Federal do Paraná,
Universidade Federal do Paraná
Caixa Postal 19044, 81531-990 Curitiba, Paraná, Brazil

Luiz G. Ferreira, and Marco A. P. Lima
Instituto de Física Gleb Wataghin,
Universidade Estadual de Campinas, UNICAMP,
13083-970 Campinas, São Paulo, Brazil

Received on 14 March, 2000

This paper is a data basis which includes tables of integral, differential, and momentum transfer cross sections for elastic electron scattering from CF_4, CCl_4, $SiCl_4$, $SiBr_4$, SiI_4, CH_3F CH_2F_2, CHF_3, CH_3Cl, CH_2Cl_2, $CHCl_3$, CF_3Cl, CF_2Cl_2, $CFCl_3$, CH_3Br, CH_3I, SiH_3Cl, SiH_3Br, SiH_3I, GeH_3Cl, GeH_3Br, SnH_3Br, C_2H_6, Si_2H_6, Ge_2H_6, B_2H_6, Ga_2H_6, H_2O, H_2S, H_2Se, H_2Te, trimethylarsine (TMAs), N_2O, and O_3. These tables show our new results, along with some of our previously published cross sections, and can easily be compared to future experimental data and other new theoretical results. Our scattering amplitudes were calculated using the Schwinger multichannel method with norm-conserving pseudopotentials. Our results are in good agreement with other theoretical data and experimental results when available.
All tables are available in the electronic version of the paper only [on the world wide web at http://www.sbf.if.usp.br/bjp/Vol31/Num1/.]

I Introduction

In this paper we show applications of the Schwinger multichannel method with norm-conserving pseudopotentials [1] to electron scattering from CF_4, CCl_4, $SiCl_4$, $SiBr_4$, SiI_4, CH_3F CH_2F_2, CHF_3, CH_3Cl, CH_2Cl_2, $CHCl_3$, CF_3Cl, CF_2Cl_2, $CFCl_3$, CH_3Br, CH_3I, SiH_3Cl, SiH_3Br, SiH_3I, GeH_3Cl, GeH_3Br, SnH_3Br, C_2H_6, Si_2H_6, Ge_2H_6, B_2H_6, Ga_2H_6, H_2O, H_2S, H_2Se, H_2Te, trimethylarsine (TMAs), N_2O, and O_3. Many of these molecules are plasma processing gases [2, 3] and some are also of environmental interest for being greenhouse gases or stratospheric ozone depleting gases [3]. Despite their industrial and environmental importance, studies on electron interactions with these molecules are very scarce. To our knowledge, this is the first collection of electron scattering cross sections for many of the molecules cited above. We intend to present in this paper a complete data base of our results, which can easily be compared to future experimental data and other new theoretical results.

In section II we present a brief review of the theory and describe the main approximations used in our calculations. In Section III we present our results and discussion. This section is divided as follows: Subsection III-1 shows our elastic differential cross sections (DCS) for CF_4, CCl_4, $SiCl_4$, $SiBr_4$ and SiI_4 from Ref. [4], in addition to results for other impact energies. We also show here our elastic integral cross sections (ICS) and unpublished momentum transfer cross

sections (MTCS) for these molecules. Subsection III-2 includes tables with elastic DCS from Ref. [5] for CH_3F CH_2F_2, CHF_3, CH_3Cl, CH_2Cl_2, $CHCl_3$, CF_3Cl, CF_2Cl_2, and $CFCl_3$ along with our results for other electron impact energies. Subsection III-3 shows our new results on elastic differential and momentum transfer cross sections for the molecules XH_3Y, with X = C, Si, Ge, Sn; Y = F, Cl, Br, I. Results of our previous studies [6] on X_2H_6 (X=C, Si, Ge) are presented in Subsection III-4. In Subsection III-5 we present our new elastic electron scattering results for Ga_2H_6 and tables with our DCS and our ICS for B_2H_6 from Ref. [6]. Our MTCS for B_2H_6, which were not included in Ref. [6] are also shown. Subsection III-6 presents our DCS for H_2X (X = O, S, Se, Te) from Ref. [7]. In Subsection III-7 we show our results for trimethylarsine (TMAs) [8]. Elastic cross sections for N_2O [9] and O_3 [10] are presented in Subsection III-8.

II Theory

The implementation of pseudopotentials in the Schwinger multichannel method allows calculations of low-energy electron scattering by molecules containing atoms with many electrons with reduced computational effort [1]. The basic idea is to replace the core electrons and the nucleus of each atom in the molecule by the corresponding soft norm-conserving pseudopotential and to describe the valence electrons in a quantum chemistry framework (Hartree-Fock approximation in the present implementation). The cross sections for electron scattering by molecules with different atoms but with the same number of valence electrons can then be calculated with about the same computational effort. To illustrate this idea, Table I shows the total number of electrons for each studied molecule compared to the number of valence electrons. The method can provide substantial computational saving, especially for molecules containing many heavier than H centers, such as $CFCl_3$ for example.

The Schwinger multichannel method has been described previously and we only review here some key features for completeness. In this method, the working expression for the scattering amplitude is

$$[f_{\vec{k}_i,\vec{k}_f}] = -\frac{1}{2\pi}\sum_{m,n}\langle S_{\vec{k}_f}|V|\chi_m\rangle(d^{-1})_{mn}\langle\chi_n|V|S_{\vec{k}_i}\rangle, \tag{1}$$

where

$$d_{mn} = \langle\chi_m|A^{(+)}|\chi_n\rangle \tag{2}$$

and

$$A^{(+)} = \frac{\hat{H}}{N+1} - \frac{(\hat{H}P + P\hat{H})}{2} + \frac{(VP+PV)}{2} - VG_P^{(+)}V. \tag{3}$$

In the above equations $|S_{\vec{k}_i}\rangle$ is the product of a target state and a plane wave, V is the interaction potential between the incident electron and the target, $|\chi_m\rangle$ is a (N+1)-electron Slater determinant used in the expansion of the trial scattering wave function, $\hat{H}$ is the total energy of the collision minus the full Hamiltonian of the system, P is a projection operator onto the open channel space defined by target eigenfunctions, and $G_P^{(+)}$ is the free-particle Green's function projected on the P-space.

In our formulation all the matrix elements needed to evaluate the scattering amplitude are computed analytically, except those involving the Green's function, *i.e.* $\langle\chi_m|VG_P^{(+)}V|\chi_n\rangle$, which are calculated by numerical quadrature [11].

We use the *norm-conserving* pseudopotentials of Bachelet Hamann and Schlüter [12] to describe the nuclear potential and the core electrons of each atom. These pseudopotentials were implemented in the SMC method as described in Ref. [1]. The Cartesian Gaussian functions used to describe the molecular and scattering orbitals were especially designed to be used in our pseudopotential calculations [13].

Our cross sections were obtained in the fixed-nuclei static-exchange approximation. We do not include the description of polarization effects, since they are known to be of little importance for the impact energy range we study here (5–30 eV). For water molecule, we also present static-exchange DCS in the (2-5)-eV energy range because, in this case, polarization effects are not so important, since the existing long–range permanent dipole moment potential is known to dominate low-energy scattering for this system [14]. We also do not include in this calculation any correction to account for the dipole potential of the polar molecules, except for the H_2X (X = O, S, Se, Te) molecules and TMAs, for which we have combined the Schwinger multichannel method with a Born closure procedure [7, 8]. The main contribution of this long range potential to the differential cross sections is at very low scattering angles, where the contribution of high partial waves is more important.

III Results and Discussion

III.1 CF_4, CCl_4, $SiCl_4$, $SiBr_4$, and SiI_4

Our elastic differential cross sections (DCS) for electron scattering from CF_4, CCl_4, $SiCl_4$, $SiBr_4$, and SiI_4 from Ref. [4] are presented in Tables II to VI, along with our results for other impact energies. Our DCS for CF_4

are in very good agreement with available experimental data [15] (see Ref. [4]). To our knowledge, except for CF_4, there are no other DCS for these molecules in the literature for comparison.

In Tables VII and VIII we show our integral elastic cross sections and our unpublished momentum transfer cross sections for CF_4, CCl_4, $SiCl_4$, $SiBr_4$, and SiI_4.

III.2 Fluoromethanes, Chloromethanes and Chlorofluoromethanes

In this subsection we present tables with our differential cross sections of Ref. [5] for CH_3F CH_2F_2, CHF_3, CH_3Cl, CH_2Cl_2, $CHCl_3$, CF_3Cl, CF_2Cl_2, and $CFCl_3$ and new results for many other electron impact energies. As an illustration, Fig. 1 compares our differential cross sections for CF_2Cl_2, CF_3Cl, CH_3Cl, and CH_2F_2 at selected impact energies with the experimental results of Ref. [16, 17, 18, 19] respectively and the agreement is very good even for impact energies as low as 5 eV. Although not shown here, our results for CH_3Cl are also in good agreement with the results obtained with the complex Kohn variational method [20] (see Ref. [5]).

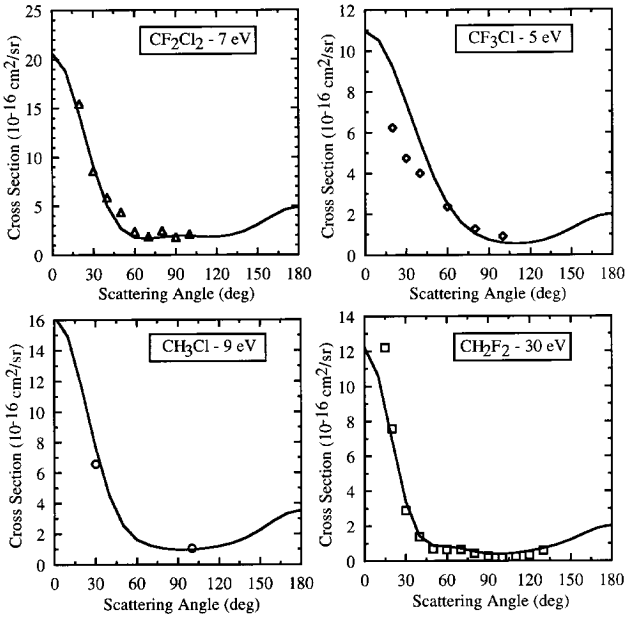

Figure 1. Our differential cross sections for selected molecules and energies compared to experimental data. Full lines: our theoretical results; triangles: CF_2Cl_2 experimental data [16]; diamonds: CF_3Cl experimental data [17]; circles: CH_3Cl experimental data [18]; squares: CH_2F_2 experimental data [19].

In Figs. 2 and 3 we compare differential cross sections for fluoromethanes and chloromethanes respectively, both at 10 eV impact energy. We also include our results for CF_4, CCl_4 and CH_4 [1]. We have shown previously [5] that the molecules with larger outer atoms present more oscillations in the differential cross sections than the other ones especially for high impact energies. This behavior indicates that the presence of larger outer atoms increases the range of the potential, and favors the coupling of higher partial waves. Figs. 2 and 3 show that this behavior is also present for lower impact energies, although less evident.

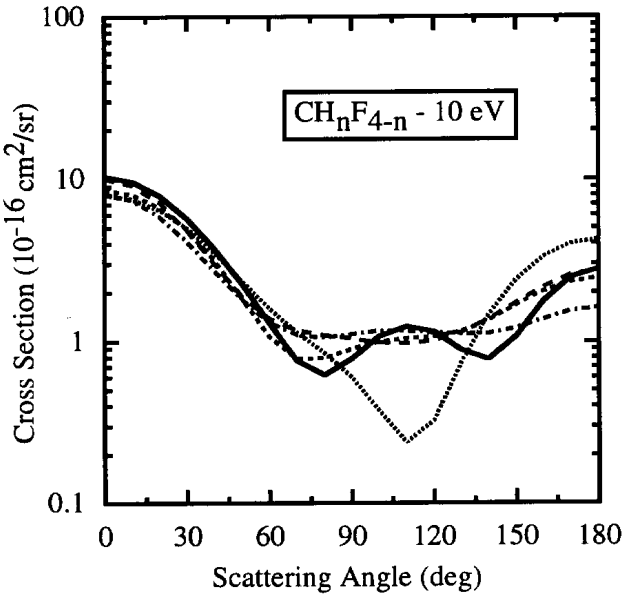

Figure 2. Differential cross sections for CH_nF_{4-n} at 10 eV. Full line: CF_4 [4]; long dashed line: CF_3H; dot–dashed line: CF_2H_2; short dashed line: CFH_3; dotted line: CH_4 [1].

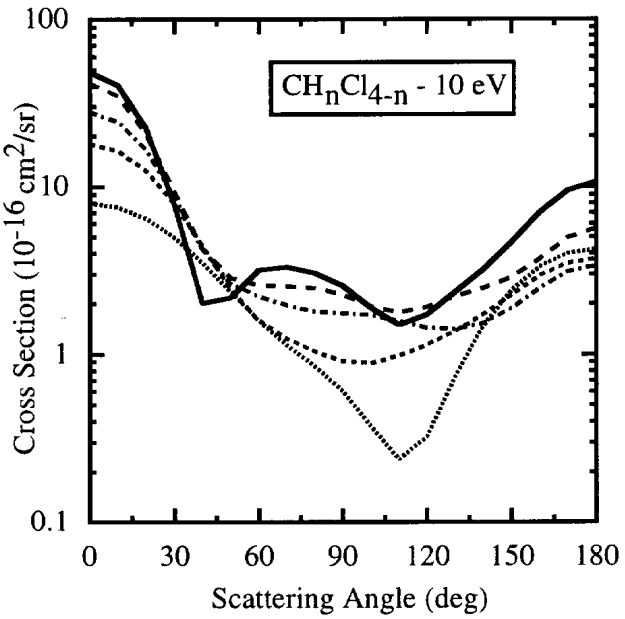

Figure 3. Differential cross sections for CH_nCl_{4-n} at 10 eV. Full line: CCl_4 [4]; long dashed line: CCl_3H; dot–dashed line: CCl_2H_2; short dashed line: $CClH_3$; dotted line: CH_4 [1].

Tables IX to XVII show our differential cross sections for CH_3F CH_2F_2, CHF_3, CH_3Cl, CH_2Cl_2, $CHCl_3$,

CF_3Cl, CF_2Cl_2, and $CFCl_3$ respectively, for several impact energies.

III.3 XH_3Y (X = C, Si, Ge, Sn; Y = F, Cl, Br, I)

In this subsection we present a comparative study of differential and momentum transfer cross sections for CH_3F, CH_3Cl, CH_3Br, CH_3I, SiH_3Cl, SiH_3Br, SiH_3I, GeH_3Cl, GeH_3Br, and SnH_3Br. To our knowledge, there are no theoretical nor experimental results for these molecules in the literature for comparison, except for CH_3F [19] and CH_3Cl [18, 20], as discussed in Subsection III-2 above.

Fig. 4 compares our differential cross sections at 20 eV for CH_3Br and CH_3I to our previous results for CH_3F, and CH_3Cl [5]. The differential cross section for CH_3F is significantly different from the results for the other molecules. CH_3Cl, CH_3Br, and CH_3I present very similar differential cross sections, with small differences only in the forward and backward directions.

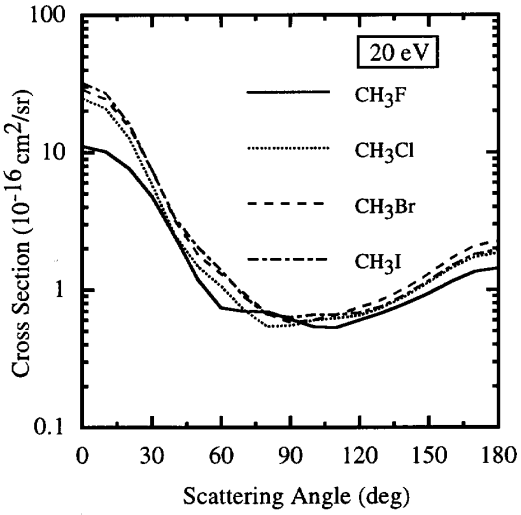

Figure 4. Differential cross sections for CH_3Y (Y = F, Cl, Br, I) at 20 eV. Full line: CH_3F [5]; dotted line: CH_3Cl [5]; dashed line: CH_3Br; dot–dashed line: CH_3I.

In Fig. 5 we compare our differential cross sections at 20 eV for SiH_3Cl, SiH_3Br, and SiH_3I (top graph) and GeH_3Cl, and GeH_3Br (bottom graph). For these two sets of molecules the peripheral atoms have little influence on the differential cross sections, except for high scattering angles.

Fig. 6 shows the influence of the central atom on the differential cross sections at 20 eV. The three pictures show that different central atoms produce little differences in the cross sections, except for CH_3I and SiH_3I (bottom graph). In this case, the presence of silicon in the molecule instead of carbon introduces undulations in the cross sections, which are characteristic of higher angular momentum coupling [5].

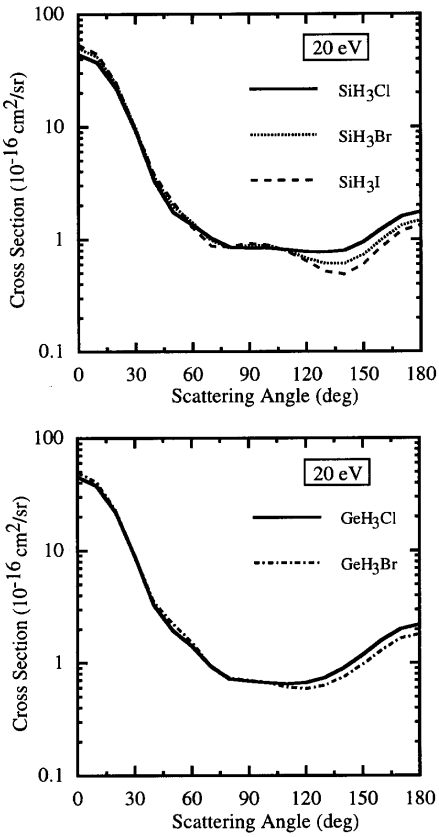

Figure 5. Differential cross sections at 20 eV. Top: results for SiH_3Y (Y = Cl, Br, I). Full line: SiH_3Cl; dotted line: SiH_3Br; dashed line: SiH_3I. Bottom: results for GeH_3Y (Y = Cl, Br). Full line: GeH_3Cl; dot–dashed line: GeH_3Br.

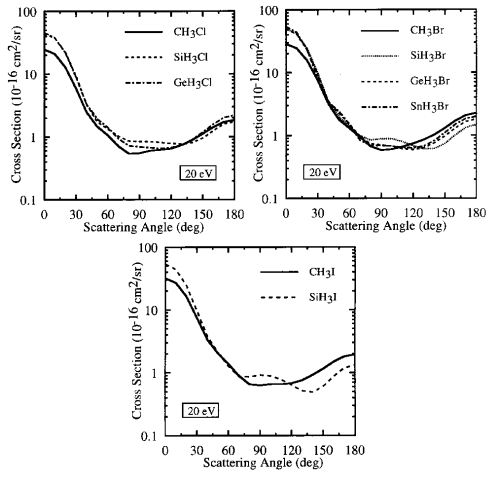

Figure 6. Differential cross sections at 20 eV. Top left: results for XH_3Cl (X = C, Si, Ge). Full line: CH_3Cl; dashed line: SiH_3Cl; dot–dashed line: GeH_3Cl. Top right: results for XH_3Br (X = C, Si, Ge, Sn). Full line: CH_3Br; dotted line: SiH_3Br; dashed line: GeH_3Br; dot-dashed line: SnH_3Br. Bottom: results for XH_3Cl (X = C, Si). Full line: CH_3Cl; dashed line: SiH_3Cl.

Tables XVIII to XXV present our differential cross sections for all the XH_3Y–type of molecules we have studied at various electron impact energies. In Table XXVI we show our results for momentum transfer

cross sections.

III.4 X_2H_6 (X=C, Si, Ge)

Elastic integral and differential cross sections for this family are presented in Tables XXVII, XXVIII and XXIX. These molecules were subject of previous studies by our group using the SMCPP method [6].

III.5 B_2H_6 and Ga_2H_6

B_2H_6 is used as gas precursor in processes of chemical vapor deposition [21] and was the subject of previous studies [6]. In this subsection we present tables with our previous results for B_2H_6 [6] and elastic electron scattering results for Ga_2H_6 for the first time. Fig. 7 shows elastic integral cross section for B_2H_6 and Ga_2H_6 from 5 eV to 30 eV. The cross section for Ga_2H_6 lies above the result for B_2H_6, and presents no structure in this energy range. The integral cross section for B_2H_6 shows a very broad feature around 10 eV.

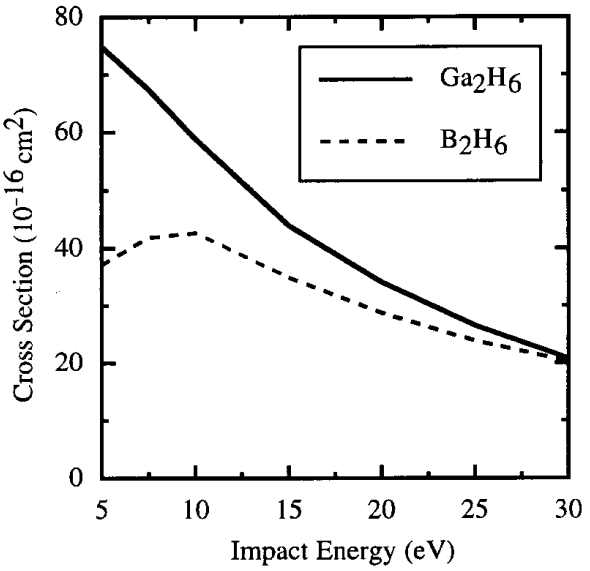

Figure 7. Elastic integral cross sections for B_2H_6 and Ga_2H_6. Solid line: Ga_2H_6; dashed line: B_2H_6.

Fig. 8 compares differential elastic cross sections for these two molecules for selected energies. These DCS are also shown in Tables XXX and XXXI along with our results for other electron impact energies. The DCS for these two molecules are dissimilar, the results for Ga_2H_6 being rich in oscillations due to higher angular momentum coupling especially at higher impact energies.

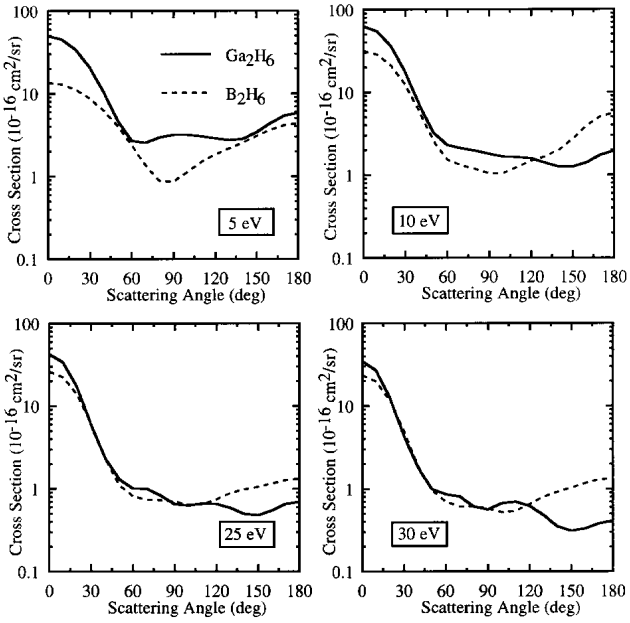

Figure 8. Differential elastic cross sections for B_2H_6 and Ga_2H_6 at 5 eV, 10 eV, 25 eV, and 30 eV. Solid lines: Ga_2H_6; dashed lines: B_2H_6.

III.6 H_2X (X = O, S, Se, Te)

In this subsection we present our elastic differential cross sections (DCS) for H_2X (X = O, S, Se, Te) from Ref. [7] (Tables XXXII to XXXV). The long–range potential due to the permanent dipole moment of the targets (H_2O and H_2S) was described through a Born closure procedure. Our DCS for H_2O and H_2S are in good agreement with available experimental data and previous calculations (see Ref. [7]). Tables with our integral cross sections and momentum transfer cross sections for these molecules are shown in Ref. [7].

III.7 $As(CH_3)_3$ – Trimethylarsine (TMAs)

The trimethylarsine molecule can be found in innumerable different conformations, since the three CH_3 groups can rotate around the As–C chemical bond. In our previous work on elastic electron scattering from TMAs [8] we have shown that, although the difference between the two selected conformations (reference conformation (RC) and lowest energy conformation (LEC)) is simply the relative positions of the hydrogen atoms, the electron scattering cross sections are sensitive to the conformation of the target for impact energies between 4 eV and 15 eV. In this energy range, one should perform an average over all possible target conformations in order to compare calculated cross sections and experimental data. Above 15 eV, however, there seems to be no relevant conformational effect.

Table XXXVI presents our differential elastic cross sections and Table XXXVII shows our elastic integral and momentum transfer cross sections for TMAs from Ref [8] at the two selected conformations.

III.8 N_2O, and O_3

In this subsection we present elastic cross sections for N_2O [9] and O_3 [10] molecules. These molecules were subject of previous studies. For O_3 we have used the first Born approximation to correct the differential cross sections at small scattering angles due to the influence of the molecular permanent dipole moment. For N_2O we have not used this procedure. In Tables XXXVIII and XXXIX we present our differential, integral and momentum transfer cross sections for N_2O and O_3 respectively at selected energies.

Tables

All tables are available only in the electronic version of the paper on the world wide web at http://www.sbf.if.usp.br/bjp/Vol31/Num1/.

Acknowledgments

A. P. P. N. acknowledges support from Fundação de Amparo à Pesquisa do Estado de São Paulo (FAPESP). M. H. F. B., L. G. F. and M. A. P. L. acknowledge partial support from Brazilian agency Conselho Nacional de Desenvolvimento Científico e Tecnológico (CNPq). M. T. N. V. acknoledges both FAPESP and CNPq. Our calculations were performed at CENAPAD-SP, at CENAPAD-NE and at CCE-UFPR.

References

[1] M. H. F. Bettega, L. G. Ferreira, and M. A. P. Lima, Phys. Rev. A **47**, 1111 (1993).

[2] M. Hayashi "Swarm Studies and Inelastic Electron-Molecule Collisions", edited by L. C. Pitchford, B. V. McKoy, A. Chutjian, and S. Trajmar, New York, p. 167 (1987).

[3] See, for example, L. G. Christophorou, J. K. Olthoff, and M. V. V. S. Rao, J. Phys. Chem. Ref. Data, **25**, 1341 (1996); L. G. Christophorou, J. K. Olthoff, and M. V. V. S. Rao, J. Phys. Chem. Ref. Data, **26**, 1 (1997); L. G. Christophorou, J. K. Olthoff, and Y. Wang, J. Phys. Chem. Ref. Data, **26**, 1205 (1997).

[4] M. T. do N. Varella, A. P. P. Natalense, M. H. F. Bettega, L. G. Ferreira, and M. A. P. Lima, Phys. Rev. A, accepted for publication (1999).

[5] A. P. P. Natalense, M. H. F. Bettega, L. G. Ferreira, and M. A. P. Lima, Phys. Rev. A, **59**, 879 (1999).

[6] M. H. F. Bettega, A. J. S. Oliveira, A. P. P. Natalense, M. A. P. Lima, L. G. Ferreira, Eur. Phys. J. D. **3**, 291 (1998).

[7] M. T. do N. Varella, M. H. F. Bettega, M. A. P. Lima, and L. G. Ferreira, J. Chem. Phys. accepted for publication (1999).

[8] M. T. do N. Varella, L. G. Ferreira, and M. A. P. Lima, J. Phys. B **32**, 2031 (1999).

[9] S. M. S. da Costa and M. H. F. Bettega, Eur. Phys. J. D **3**, 67 (1998).

[10] M. H. F. Bettega, M. T. do N. Varella, M. A. P. Lima, and L. G. Ferreira, J. Phys. B **31**, 4419 (1998).

[11] M. A. P. Lima, L. M. Brescansin, A. J. R. da Silva, C. Winstead, and V. McKoy, Phys. Rev. A **41**, 327 (1990).

[12] G. B. Bachelet, D. R. Hamann, and M. Schlüter, Phys. Rev. B **26**, 4199 (1982).

[13] M. H. F. Bettega, A. P. P. Natalense, M. A. P. Lima, and L. G. Ferreira, Int. J. Quantum Chem., **60**, 821 (1996).

[14] T. N. Rescigno and B. H. Lengsfield, Z. Phys. D **24**, 117 (1992).

[15] L. Boesten, H. Tanaka, A. Kobayashi, M. A. Dillon, and M. Kimura, J. Phys. B **25**, 1607 (1992).

[16] A. Mann, and F. Linder, J. Phys. B, **25**, 1633 (1992).

[17] A. Mann, and F. Linder, J. Phys. B, **25**, 1621 (1992).

[18] X. Shi, V. K. Chan, G. A. Gallup, and P. D. Burrow, J. Chem. Phys., **104**, 1855 (1996).

[19] H. Tanaka, T. Masai, M. Kimura, T. Nishimura, and Y. Itikawa, Phys. Rev. A **56**, R3338 (1997).

[20] T. N. Rescigno, A. E. Orel, and C. W. McCurdy, Phys. Rev. A, **56**, 2855, (1997).

[21] I. Konyashin, J. Bill, and F. Aldinger, Chem. Vap. Deposition **3**, 239 (1997).